Measurement of transition quadrupole moments of high-spin states in the N = 74 isotones ^{133}Pr, ^{132}Ce and ^{131}La

E.S. Paul,[1][*] S.A. Forbes,[1] J. Gizon[2], K. Hauschild,[3][†] I.M. Hibbert,[3][‡] D.T. Joss,[1][§]

P.J. Nolan,[1] B.M. Nyakó,[4] J.A. Sampson,[1] A.T. Semple,[1] R. Wadsworth,[3] L. Walker,[1] J.N. Wilson[1][**] and L. Zolnai[4]

[1] *Oliver Lodge Laboratory, University of Liverpool, PO Box 147, Liverpool L69 7ZE, United Kingdom*

[2] *Institut des Sciences Nucléaires, IN2P3-CNRS/Université Joseph Fourier, Grenoble, France*

[3] *Department of Physics, University of York, Heslington, York YO1 5DD, United Kingdom*

[4] *Institute of Nuclear Research, H-4001 Debrecen, Hungary*

(December 5, 2000)

Abstract

The Doppler Shift Attenuation Method has been used to extract transition quadrupole moments of high-spin bands in the N = 74 isotones ^{133}Pr, ^{132}Ce and ^{131}La, produced in the ^{37}Cl + ^{100}Mo reaction. The results appear to be configuration dependent and, for ^{133}Pr and ^{132}Ce, the involvement of $\Omega = 1/2$

[*]E-mail: esp@ns.ph.liv.ac.uk

[†]Present address: DAPNIA/SPhN CEA Saclay, Bat 703 l'Orme des Merisiers, F-91191 Gif-sur-Yvette, France

[‡]Present address: Oliver Lodge Laboratory, University of Liverpool, PO Box 147, Liverpool L69 7ZE, United Kingdom

[§]Present address: School of Sciences, Staffordshire University, Stoke on Trent ST4 2DE

[**]Present address: Niels Bohr Institute, Blegdamsvej 17 Dk-2100 Copenhagen, Denmark

$\nu h_{9/2}$ and $\nu f_{7/2}$ intruder orbitals appears to enhance the collectivity at high spin ($I > 25\hbar$).

PACS numbers: 21.10.Re, 27.60+q, 23.20.Lv.

Typeset using REVTEX

Nuclear reactions, ^{37}Cl+^{100}Mo at 155 MeV, enriched targets, Eu-
ROGAM spectrometer array of HPGe detectors, measured fractional
Doppler shifts, deduced Q_t, quadrupole deformations.

I. INTRODUCTION

Nuclei near N = 74 in the light rare-earth region (A $\sim$ 130) are ideal for studying the core-polarising effects of specific nuclear quasiparticle configurations. These nuclei are well known to possess shallow potential energy surfaces with respect to both quadrupole deformation β_2, leading to the observation of high-spin superdeformed[1] bands, and triaxiality γ, leading to prolate/oblate shape coexistence. This is illustrated in Fig. 1, which shows results from theoretical Total Routhian Surface (TRS) calculations [1–3] for ^{133}Pr. Minima are evident for $\beta_2 \approx 0.2$ with γ near +30°, −30° and −60°, while a superdeformed prolate ($\gamma = 0°$) minimum can also be seen for $\beta_2 \gtrsim 0.35$. Each energy minimum is built on a different underlying multiquasiparticle configuration and it is therefore important to extract nuclear deformations, particularly at high spin, for these coexisting structures, in order to test the predictive power of nuclear models in this mass region. This may be achieved by measuring mean nuclear level lifetimes, using the Doppler Shift Attenuation Method (DSAM) [4], and extracting transition quadrupole moments. It is also important to study many configurations/nuclei under identical experimental conditions and to follow a consistent analysis procedure in order to remove systematic errors associated with poor knowledge of nuclear stopping powers. This has been achieved in the present work by using a single reaction together with a powerful γ-ray spectrometer to select bands in the residual nuclei by multiple γ-ray gating. Indeed, the present paper reports on lifetime measurements at high spin in the N = 74 isotones ^{133}Pr, ^{132}Ce and ^{131}La. Results of previous high-spin studies of these nuclei can be found in Refs. [5–7].

II. EXPERIMENTAL DETAILS

High-spin states in ^{133}Pr, ^{132}Ce and ^{131}La were populated using the ^{37}Cl + ^{100}Mo reaction, carried out at the Centre de Recherches Nucléaires, Strasbourg. The Vivitron electrostatic accelerator provided a 155 MeV ^{37}Cl beam to bombard a target consisting of 550 μg/cm^2 of ^{100}Mo backed by 15 mg/cm^2 of gold. Coincident escape-suppressed, high-fold γ-ray events (γ^n, $n \geq 5$) were collected using the EUROGAM II spectrometer [8] which contained 54

---

[1]In this mass region the term 'superdeformed' has been applied to prolate shapes with a major to minor axis ratio of 3:2, corresponding to $\beta_2 \approx 0.35 - 0.40$.

HPGe detectors including 24 "clover" detectors [9], each of which consists of four separate Ge crystals. A total of 1.5×10^8 events were recorded to tape for subsequent analysis. The three nuclei ^{133}Pr, ^{132}Ce and ^{131}La were populated through 4n, p4n and α2n evaporation from the compound ^{137}Pr* system, respectively, and were measured to be populated in the ratio 10:6:1, approximately.

III. DATA ANALYSIS

A γ ray that is emitted while the recoiling nucleus is slowing down in the target and backing material will exhibit a Doppler shifted, and broadened, lineshape. The magnitude of the shift is related to the mean lifetime of the depopulated and feeding levels, together with the stopping powers of the slowing down medium. A measurement of the centroid shift of γ rays can thus be used to extract mean level lifetimes by modelling the slowing down process. Since an inherent systematic uncertainty of 10–15% occurs for stopping powers, it is important to measure several bands/nuclei under the same experimental conditions to provide good relative results. Such measurements have already been applied to this mass region, particularly for superdeformed bands [10–12].

Asymmetric DSAM matrices were constructed from the present data, gated by low-spin transitions in a particular band/nucleus. These matrices contained detectors located at a forward angle of the EUROGAM spectrometer (a ring of ten at $\theta = 46.4°$) sorted against all angles, and detectors located at the complementary backward angle (a ring of ten at $\theta = 133.6°$) sorted against all angles. Gamma-ray spectra were then generated by projecting onto the forward and backward angles of these matrices, respectively, such that the resulting 1D spectra were double-gated by γ rays. Again the low-spin fully stopped transitions were used as the gates. This method allows side-feeding into the levels which could effect the results. In the case of superdeformed bands in this mass region, then if the sidefeeding is eliminated by gating above the level of interest, a 10% increase in extracted quadrupole moments has been found [10,12]. A lack of statistics in the present data together with the lower number of available gates precluded a similar analysis here.

Two methods of background subtraction were tried. In the first method, a fraction of the total projection onto the forward/backward axes of the DSAM matrices was used as the background spectrum; in the second method, the DSAM matrices were themselves background subtracted, using the technique of Ref. [13], prior to the final gating. No significant

difference was found, however, in the quality of the final spectra.

To first order, the Doppler-shifted energy of a transition E_0 measured at an angle θ is,

$$E(\theta) = E_0 \left[1 + F(\tau)\frac{v_0}{c} \cos(\theta) \right], \tag{1}$$

where $F(\tau) = \langle v(t) \rangle / v_0$ is the fractional Doppler shift factor. Experimental $F(\tau)$ factors were calculated by estimating the centroid shift,

$$\Delta E = \frac{1}{2} \left[E(\theta = 46.4°) - E(\theta = 133.6°) \right], \tag{2}$$

for each transition in a particular band. Theoretical $F(\tau)$ curves, corresponding to different (constant) values of the transition quadrupole moment, Q_t, were generated for a particular band in a nucleus and compared to the experimental $F(\tau)$ values of that band. These calculations are the same as reported in Ref. [10] and used Ziegler stopping powers [14] to evaluate the slowing down process of the recoiling nuclei in the target and backing material. The average initial recoil velocity v_0 was calculated assuming production at the target midpoint and the recoil was assumed to move along the beam axis.

IV. EXPERIMENTAL RESULTS

A. ^{133}Pr

A partial decay scheme of ^{133}Pr is shown in Fig. 2. In addition to the bands shown in the figure, several strongly coupled $\Delta I = 1$ bands were observed; these will be discussed elsewhere [15]. The topmost transitions of bands 2 and 3, together with the newly identified band 4, were observed in the data of Ref. [16], which used a thin target. The spin and parity assignments shown in Fig. 2 reflect results from an angular correlation analysis of this data set.

Forward- and backward-angle spectra for the $(\pi,\alpha) = (-,-1/2)$ band 1 are shown in Fig. 3(a). The 863-865-867 keV triplet and the 922 keV transition exhibit lineshapes with an appreciable stopped component. However, the higher-spin transitions exhibit only Doppler shifted components, allowing a simple centroid-shift analysis to be applied; the results are included in Fig. 3(b). Except for the first transition (990 keV), band 1 exhibits a quadrupole moment of $Q_t \approx 4.5$ eb. Since bands 2 and 3 are signature partners, both bands can be compared to the same theoretical curves, which depend on the spin-energy characteristics of

the band. Hence the results for bands 2 and 3 are shown together in Fig. 3(b), but separately to band 1. Bands 2 and 3 appear to have a smaller quadrupole moment $Q_t \approx 2.5 - 3.0$ eb at low spin, but at higher spin there is evidence for an increase in Q_t beyond 3.0 eb. Taken together, the results for bands 1–3 suggest an increase in quadrupole moment at $I \approx 25\hbar$ (or frequency ω_{ef}, see Section V A 1) as indicated in Fig. 3(b).

B. ^{132}Ce

A partial decay scheme of ^{132}Ce [6] is shown in Fig. 4(a), while the fractional Doppler shift factors are shown in Fig. 4(b). Bands 1–3 have a transition quadrupole moment of $Q_t \approx 3.0$ eb at low spin but band 1 appears to have a larger quadrupole moment, $Q_t \approx 3.5 - 4.0$ eb at high spin.

C. ^{131}La

A partial decay scheme of ^{131}La [17] is shown in Fig. 5(a). The spin and parity assignments follow from an angular correlation analysis of the present data. Unlike the ^{133}Pr isotone (Fig. 2), the positive-parity bands 2 and 3 dominate at high spin and it was only possible to extract a quadrupole moment for the $(\pi,\alpha) = (+,-1/2)$ band 2. The fractional Doppler shift factors are shown in Fig. 5(b) where a value of $Q_t \approx 2.3$ eb is found for band 2.

V. DISCUSSION

In order to compare experimental (Q_t) and theoretical (β_2, γ) quantities, the following relations are used [18,19]:

$$Q_t = Q_{20} \frac{\cos(\gamma + 30^\circ)}{\cos(30^\circ)}, \tag{3}$$
$$Q_{20} = 0.0109 Z A^{2/3} \beta_2 \left(1 + 0.36\beta_2\right).$$

These equations neglect higher order deformations such as hexadecapole deformation β_4.

A. ^{133}Pr

1. Band configurations

The alignments i_x [20] of the bands in ^{133}Pr are plotted as a function of rotational frequency in Fig. 6(a). A rotational reference, with a variable moment of inertia $\mathcal{J}_{ref} = \mathcal{J}_0 + \omega^2 \mathcal{J}_1$, has been subtracted with Harris parameters [21] $\mathcal{J}_0 = 17\hbar^2 \text{MeV}^{-1}$ and $\mathcal{J}_1 = 25\hbar^4 \text{MeV}^{-3}$. In the standard notation, band 1 is built on orbital E ($\pi h_{11/2}$) at low spin and backbends into the EFG ($\pi[h_{11/2}^3]$) 3-quasiproton configuration at higher spin, or rotational frequency $\omega_{FG} \approx 0.44$ MeV/$\hbar$. Bands 5 and 6 are signature partners, B and A, derived from a $\pi g_{7/2}$ orbital, which backbend at $\omega_{EF} \approx 0.28$ MeV/$\hbar$ into bands 2 and 3, respectively, based on BEF and AEF 3-quasiproton configurations ($\pi[g_{7/2}h_{11/2}^2]$). Bands 1, 2 and 3 all show a gradual increase in alignment at the highest spins which can be attributed to ef neutrons (of mixed $\nu h_{11/2}$, $\nu h_{9/2}$ and $f_{7/2}$ parentage). Band 4, newly identified, is probably built on the DEF configuration ($\pi[d_{5/2}h_{11/2}^2]$); a $\pi d_{5/2}$ orbital also forms the $3/2^+$ ground state of ^{133}Pr [22]. Three sidebands (AE, BE and DE) are also observed in the ^{132}Ce core [6] and the three positive-parity bands in ^{133}Pr are formed by adding the extra proton in orbit F. The band assignments and rotational alignments in ^{133}Pr are summarised in Fig. 6(a).

Calculations suggest that ^{133}Pr is γ-soft (see Fig. 1). An experimental handle on this is the energy splitting in signature-partner bands, i.e. the positive-parity bands in ^{133}Pr. A quantity that enhances the signature splitting is the staggering parameter $S(I)$:

$$S(I) = E(I) - E(I-1) - \frac{1}{2}\left[E(I+1) - E(I) + E(I-1) - E(I-2)\right]. \qquad (4)$$

This is plotted in Fig. 6(b) for the positive-parity signature-partner bands 5/6 and 2/3. The magnitude of the staggering parameter increases up to the backbend; it then decreases and changes sign again at $I \approx 20\hbar$. This behaviour may indicate that the shape (γ deformation) is changing as the spin increases. Moreover, as in the ^{132}Ce core, the nonobservation of orbital C, the second proton orbital with parity and signature $(\pi,\alpha) = (+,+1/2)$, is suggestive of triaxiality [6].

2. Quadrupole moments

Apart from the lowest-spin point at $I \approx 23\hbar$, the transition quadrupole moment extracted for band 1 is $Q_t \approx 4.5$ eb. This value translates into a quadrupole deformation $\beta_2 \approx 0.25$ for

an axially symmetric prolate nuclear shape ($\gamma = 0°$). However, results of TRS calculations for the EFG configuration ($\pi[h_{11/2}^3]$) suggest a significant triaxiality at high spin with γ near $-30°$. With such triaxiality, the experimental quadrupole deformation reduces to $\beta_2 \approx 0.22$ (equation 3), which is still slightly higher than the TRS predictions of $\beta_2 = 0.20$.

The quadrupole moments extracted for bands 2 and 3 in the spin range $I \approx 21 - 25\hbar$ appear lower than band 1, and average around $Q_t = 2.75$ eb. This value translates into a quadrupole deformation $\beta_2 \approx 0.17$ for a prolate nuclear shape, or $\beta_2 \approx 0.14$ for $\gamma = -30°$. However, there appears to be an increase in Q_t with the highest points for bands 2 and 3 increasing beyond $Q_t = 3.0$ eb. Indeed, all three bands show an increase in Q_t, and hence collectivity, at $I \approx 25\hbar$, which corresponds to the frequency of the onset of the gradual alignment of neutrons evident in Fig. 6(a).

The occupation of shape-driving low-Ω $\nu h_{9/2}/f_{7/2}$ orbitals from above the N = 82 spherical shell gap could explain the increase in collectivity. Moreover, bands in odd-odd ^{132}Pr and ^{130}Pr, that involve these neutron orbitals, have similarly been measured to possess enhanced quadrupole moments [11]. TRS calculations for the EFGef 5-quasiparticle configuration show a shallow energy minimum at $I \sim 25\hbar$ with $\beta_2 = 0.243$ and $\gamma = 4°$, which results in a theoretical quadrupole moment close to the experimental value for band 1 of $Q_t \approx 4.5$ eb. This "enhanced" deformation minimum is still somewhat lower in deformation than the "superdeformed" minimum at $\beta_2 \approx 0.37$, shown in Fig. 1.

The results of cranking calculations, employing a triaxial Woods-Saxon single-particle potential [23,24], are shown in Fig. 7 corresponding to the TRS enhanced deformation minimum. Several $\Omega = 1/2$ quasineutron orbitals are strongly lowered in energy with increasing rotational frequency, namely the negative-parity orbitals labelled g and h, and the positive-parity orbital labelled 6_1. The g and h orbitals are derived from mixed $\nu f_{7/2}$ ($[530]1/2^-$) and $\nu h_{9/2}$ ($[541]1/2^-$) states, while the 6_1 orbital is derived from the first state of the N_{osc} = 6 oscillator shell ($[660]1/2^+$). All three orbitals originate from above the spherical N = 82 spherical shell gap and are strongly shape-driving to increased prolate quadrupole deformation, i.e. $\partial E/\partial \beta_2 \ll 0$. The g and h orbitals are seen to interact with and cross the degenerate e and f orbitals ($[514]9/2^-$, $\alpha = \pm 1/2$) at $\omega \approx 0.45$ MeV/$\hbar$ and then align at $\omega_{ef} \approx 0.55$ MeV/$\hbar$ causing the gradual increase in i_x evident in Fig. 6(a), together with the inversion of the staggering parameter for bands 2 and 3 seen in Fig. 6(b). The occupation of the g and/or h orbitals would stabilise the enhanced deformation at high spin. Four superdeformed bands have already been assigned to this nucleus [16] but are thought to

involve other shape-driving orbitals, namely $i_{13/2}$ neutrons (the 6_1 intruder of Fig. 7) [2] and $g_{9/2}$ proton-holes [25,26].

B. ^{132}Ce

1. Band configurations

Experimental alignments are shown in Fig. 8(a) together with band assignments. Band 1, the S band, is based on the 2-quasiproton EF $(\pi[h^2_{11/2}])$ configuration at low spin, while bands 2–4 correspond to negative-parity BE, AE and DE 2-quasiproton configurations $(\pi[g_{7/2}h_{11/2}]$ and $\pi[d_{5/2}h_{11/2}])$, respectively. The staggering parameter for bands 2 and 3 is shown in Fig. 8(b). Similar to ^{133}Pr, the magnitude of the staggering parameter decreases with increasing spin but then starts to increase again above spin $I = 16\hbar$.

2. Quadrupole moments

Similar to ^{133}Pr, the quadrupole moments extracted for band 1 in ^{132}Ce appear higher at high spin $(Q_t \approx 3.5 - 4.0$ eb$)$ than at low spin $(Q_t \approx 3.0$ eb$)$. Again the increase can be attributed to the involvement of the low-Ω $\nu h_{9/2}/f_{7/2}$ orbitals at ω_{ef} in Fig. 8(a). The high-spin values correspond to a deformation $\beta_2 \approx 0.21 - 0.23$ assuming axial symmetry $(\gamma = 0°)$. Only one point each could be measured for the negative-parity bands 2 and 3 in ^{132}Ce; values of $Q_t \approx 2.75$ eb were found, similar to bands 2 and 3 in ^{133}Pr.

It was also possible from the present data to extract an approximate Q_t value for the first superdeformed band in ^{132}Ce; a value of $Q_t \sim 7.0$ eb was found. This value is consistent with precise measurements [10] obtained with the GAMMASPHERE spectrometer and provides a calibration of the present analysis.

C. ^{131}La

1. Band configurations

The structure of odd-Z ^{131}La [17] appears similar to odd-Z ^{133}Pr. Experimental alignments for the corresponding bands 1–3 in ^{131}La are shown in Fig. 9(a) together with band

assignments. Again, band 1 is built on orbital E ($\pi h_{11/2}$) at low spin and backbends into the EFG ($\pi[h_{11/2}^3]$) 3-quasiproton configuration at higher spin. Bands 2 and 3, are based on BEF and AEF 3-quasiproton ($\pi[g_{7/2}h_{11/2}^2]$) configurations, respectively. In contrast to ^{133}Pr, however, the positive-parity bands 2 and 3 dominate at high spin. The behaviour of these bands at high spin has been interpreted as a form of smooth band termination [17], involving a gradual shape change from prolate to oblate over several transitions.

The staggering parameter for bands 2 and 3 is shown in Fig. 9(b). Similar to ^{133}Pr and ^{132}Ce, the magnitude of the staggering parameter decreases with increasing spin up to $16\hbar$. However, there is no inversion and the magnitude increases again above spin $I \approx 17\hbar$.

2. Quadrupole moments

The transition quadrupole moment, $Q_t \approx 2.3$ eb, extracted for band 2 in the spin range $I \approx 22 - 28\hbar$, translates into a quadrupole deformation $\beta_2 \approx 0.14$ for an axially symmetric prolate nuclear shape ($\gamma = 0°$). The relatively low Q_t value could also imply significant triaxiality with $\gamma > 0°$, as expected for the beginning of a smoothly terminating band.

VI. CONCLUSIONS

Transition quadrupole moments have been extracted for several bands in the N = 74 isotones ^{133}Pr, ^{132}Ce and ^{131}La in a consistent manner. In ^{133}Pr, there is evidence for an increase in collectivity around spin $I = 25\hbar$. Above this spin, the negative-parity yrast band exhibits a quadrupole moment $Q_t \approx 4.5$ eb, which is unusually large for a "normally deformed" (i.e. not superdeformed) band in this mass region. The appearance of shape-driving $\nu h_{9/2}/f_{7/2}$ orbitals at the Fermi surface at high spin could be responsible for the enhanced collectivity. A similar increase in collectivity is observed in the S-band of ^{132}Ce, which can again be related to the influence of low-Ω $\nu h_{9/2}/f_{7/2}$ intruders.

The smallest quadrupole moment was found for the $(\pi,\alpha) = (+,-1/2)$ band in ^{131}La. This is however consistent with the recent interpretation of this band as an example of a smoothly terminating band [17]. Low collectivity is expected for shapes with $\gamma > 0°$.

VII. ACKNOWLEDGEMENTS

REFERENCES

[1] W. Nazarewicz, G.A. Leander and J. Dudek, Nucl. Phys. A 467 (1987) 437.

[2] R. Wyss, J. Nyberg, A. Johnson, R. Bengtsson and W. Nazarewicz, Phys. Lett. B 215 (1988) 211.

[3] W. Nazarewicz, R. Wyss and A. Johnson, Nucl. Phys. A 503 (1989) 285.

[4] P.J. Nolan and J.F. Sharpey-Schafer, Rep. Prog. Phys. 42 (1979) 1.

[5] L. Hildingsson, C.W. Beausang, D.B. Fossan and W.F. Piel, Jr., Phys. Rev. C 37 (1988) 985.

[6] E.S. Paul, A.J. Boston, D.T. Joss, P.J. Nolan, J.A. Sampson, A.T. Semple, F. Farget, A. Gizon, J. Gizon, D. Santos, B.M. Nyakó, N.J. O'Brien, C.M. Parry and R. Wadsworth, Nucl. Phys. A 619 (1997) 177.

[7] L. Hildingsson, C.W. Beausang, D.B. Fossan, R. Ma, E.S. Paul, W.F. Piel, Jr. and N. Xu, Phys. Rev. C 39 (1989) 471.

[8] C.W. Beausang and J. Simpson, J. Phys. G 22 (1996) 527.

[9] P.M. Jones, L. Wei, F.A. Beck, P.A. Butler, T. Byrski, G. Duchêne, G. deFrance, F. Hannachi, G.D. Jones and B. Kharraja, Nucl. Instrum. and Methods A 362 (1995) 556.

[10] R.M. Clark, I.Y. Lee, P. Fallon, D.T. Joss, S.J. Asztalos, J.A. Becker, L. Bernstein, B. Cederwall, M.A. Deleplanque, R.M. Diamond, L.P. Farris, K. Hauschild, W.H. Kelly, A.O. Macchiavelli, P.J. Nolan, N. O'Brien, A.T. Semple, F.S. Stephens and R. Wadsworth, Phys. Rev. Lett. 76 (1996) 3510.

[11] F.G. Kondev, M.A. Riley, D.J. Hartley, T.B. Brown, R.W. Laird, M. Lively, J. Pfohl, R.K. Sheline, R.M. Clark, P. Fallon, D.G. Sarantites, M. Devlin, D.R. LaFosse, F. Lerma, R. Wadsworth, I.M. Hibbert, N.J. O'Brien, E.S. Paul, D.T. Joss, P.J. Nolan, S.L. Shepherd and J. Simpson, Phys. Rev. C 59 (1999) 3076.

[12] F.G. Kondev, M.A. Riley, D.J. Hartley, T.B. Brown, R.W. Laird, M. Lively, R.K. Sheline, E.S. Paul, D.T. Joss, P.J. Nolan, S.L. Shepherd, R.M. Clark, P. Fallon, D.G. Sarantites, M. Devlin, D.R. LaFosse, F. Lerma, R. Wadsworth, I.M. Hibbert, N.J.

O'Brien and J. Simpson, Phys. Rev. C 60 (1999) 011303.

[13] G. Palameta and J. Waddington, Nucl. Instrum. and Methods A234 (1985) 476.

[14] J.F. Ziegler, *The Stopping and Ranges of Ions in Matter* (Pergamon, London, 1985), Vols. 3 and 5.

[15] E.S. Paul, D.M. Cullen, S.A. Forbes, J. Gizon, K. Hauschild, I.M. Hibbert, D.T. Joss, P.J. Nolan, B.M. Nyakó, J.A. Sampson, A.T. Semple, R. Wadsworth, L. Walker, J.N. Wilson and L. Zolnai, to be published.

[16] J.N. Wilson, P.J. Nolan, C.W. Beausang, R.M. Clark, S.A. Forbes, A. Gizon, J. Gizon, K. Hauschild, I.M. Hibbert, E.S. Paul, D. Santos, A.T. Semple, J. Simpson and R. Wadsworth, Phys. Rev. Lett. 74 (1995) 1950.

[17] R. Wadsworth, E.S. Paul, A. Astier, D. Bazzacco, A.J. Boston, N. Buforn, C.J. Chiara, D.B. Fossan, C. Fox, J. Gizon, D.G. Jenkins, N.S. Kelsall, T. Koike, D.R. LaFosse, S. Lunardi, P.J. Nolan, B.M. Nyakó, C.M. Petrache, H.C. Scraggs, K. Starosta, J. Timár, A. Walker, A.N. Wilson, L. Zolnai, B.G. Dong and I. Ragnarsson, Phys. Rev. C 62 (2000) 034315.

[18] P. Ring, A Hayashi, K. Hara, H. Emling and E. Grosse, Phys. Lett. B110 (1982) 423.

[19] W. Nazarewicz and I. Ragnarsson *Nuclear Deformation, in Handbook on Nuclear Properties*, eds. D.N. Poenaru and W. Greiner (Clarendon Press, Oxford, 1996) p. 80.

[20] R. Bengtsson and S. Frauendorf, Nucl. Phys. A 327 (1979) 139.

[21] S.M. Harris, Phys. Rev. 138 (1965) B509.

[22] C.F. Liang, P. Paris, D. Bucurescu and M.S. Rapaport, Phys. Rev. C 40 (1989) 2796.

[23] W. Nazarewicz, J. Dudek, R. Bengtsson and I. Ragnarsson, Nucl. Phys. A 435 (1985) 397.

[24] S. Cwiok, J. Dudek, W. Nazarewicz, W. Skalski and T. Werner, Comp. Phys. Comm. 46 (1987) 379.

[25] A. Galindo-Uribarri, D. Ward, T. Drake, G. Hackman, V.P. Janzen, S.M. Mullins, S. Pilotte, D.C. Radford, I. Ragnarsson, N.C. Schmeing and J.C. Waddington, Phys. Rev. C 50 (1994) R2655.

[26] A. Galindo-Uribarri, D. Ward, H.R. Andrews, G.C. Ball, D.C. Radford, V.P. Janzen, S.M. Mullins, J.C. Waddington, A.V. Afanasjev and I. Ragnarsson Phys. Rev. C 54 (1996) R1057.
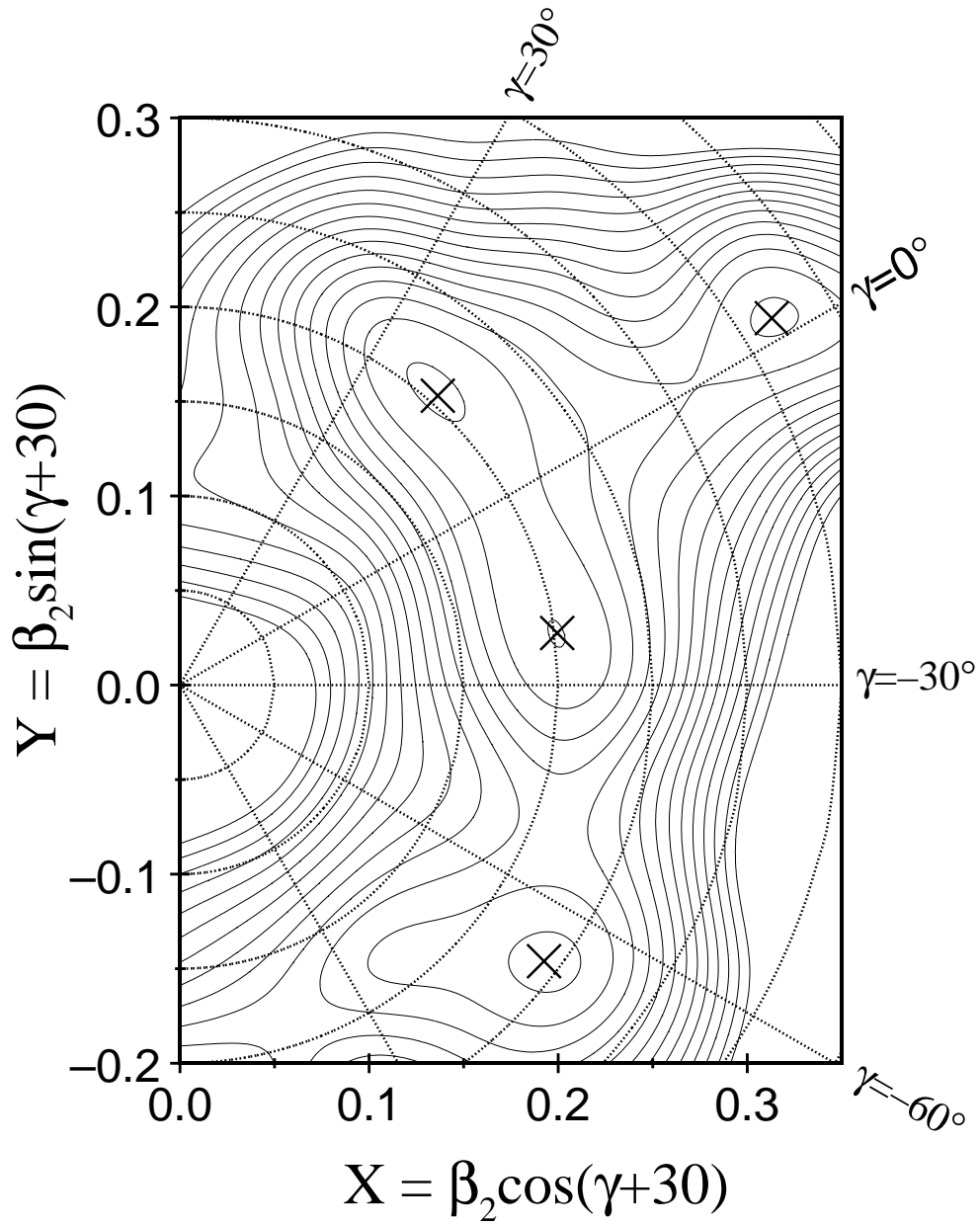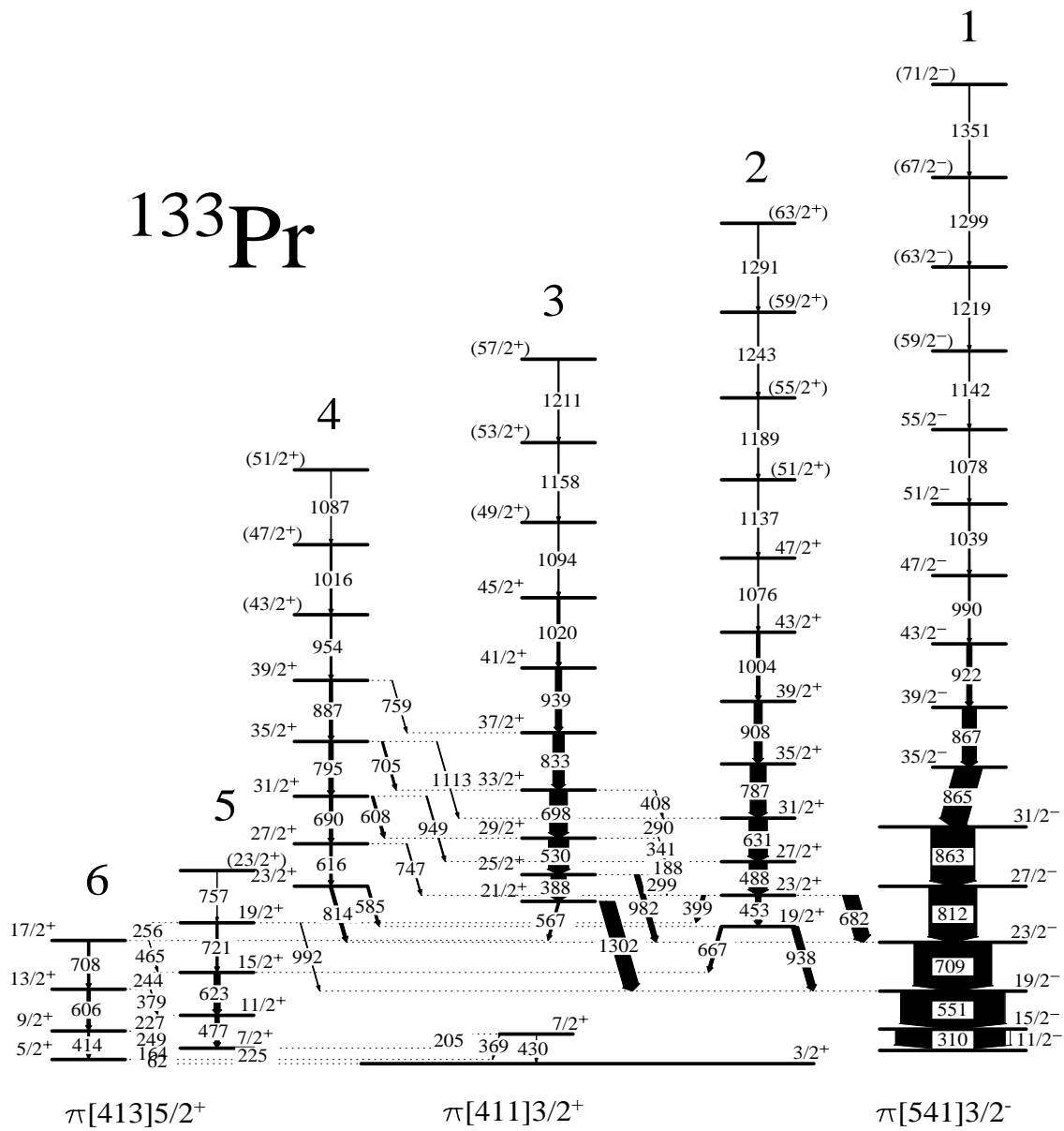
Fig. 1

FIG. 1. Representative TRS calculations for ^{133}Pr at $\omega = 0.47$ MeV$/\hbar$. Several coexisting local minima, denoted by crosses, are evident. The energy contours are separated by 150 keV.

$^{133}\mathrm{Pr}$

1

2

3

4

5

6

$(71/2^-)$
1351
$(67/2^-)$
1299
$(63/2^-)$
1219
$(59/2^-)$
1142
$55/2^-$
1078
$51/2^-$
1039
$47/2^-$
990
$43/2^-$
922
$39/2^-$
867
$35/2^-$
865
$31/2^-$
863
$27/2^-$
812
$23/2^-$
709
$19/2^-$
551
$15/2^-$
310
$11/2^-$

$(63/2^+)$
1291
$(59/2^+)$
1243
$(55/2^+)$
1189
$(51/2^+)$
1137
$47/2^+$
1076
$43/2^+$
1004
$39/2^+$
908
$35/2^+$
787
$31/2^+$
631
$27/2^+$
488
$23/2^+$
453
$19/2^+$
682
938
667
399
982
1302
299
188
341
290
408

$(57/2^+)$
1211
$(53/2^+)$
1158
$(49/2^+)$
1094
$45/2^+$
1020
$41/2^+$
939
$37/2^+$
833
$33/2^+$
698
$29/2^+$
530
$25/2^+$
388
$21/2^+$
567
1113
949
747
705
759
608

$(51/2^+)$
1087
$(47/2^+)$
1016
$(43/2^+)$
954
$39/2^+$
887
$35/2^+$
795
$31/2^+$
690
$27/2^+$
616
$23/2^+$
757
$19/2^+$
585
814

$(23/2^+)$
721
$15/2^+$
623
$11/2^+$
477
$7/2^+$
225
992
256
244
379
227
249
164
82

$17/2^+$
708
$13/2^+$
606
$9/2^+$
414
$5/2^+$
465

$7/2^+$
205
369
430
$3/2^+$

$\pi[413]5/2^+$

$\pi[411]3/2^+$

$\pi[541]3/2^-$

Fig. 2

FIG. 2. Partial level scheme deduced for $^{133}\mathrm{Pr}$ from this work. The transition energies are given in keV and their relative intensities are proportional to the widths of the arrows. Nilsson orbital assignments at low spin are also labelled.
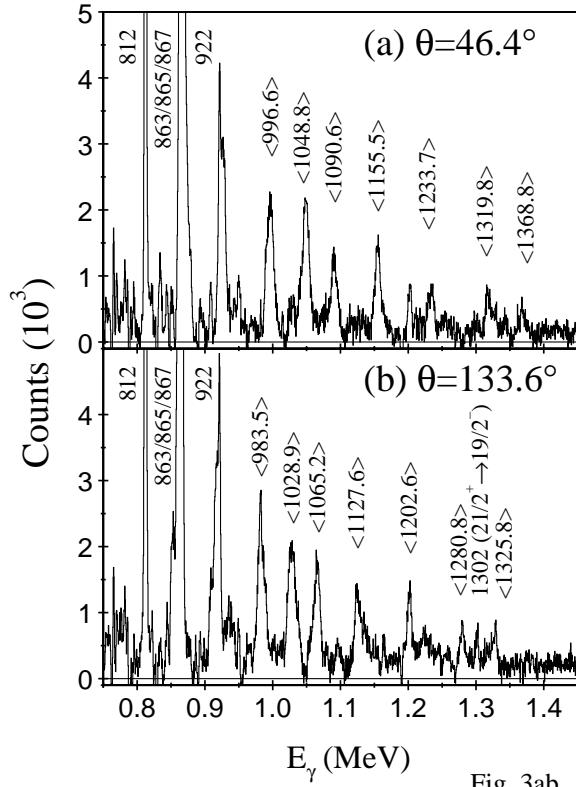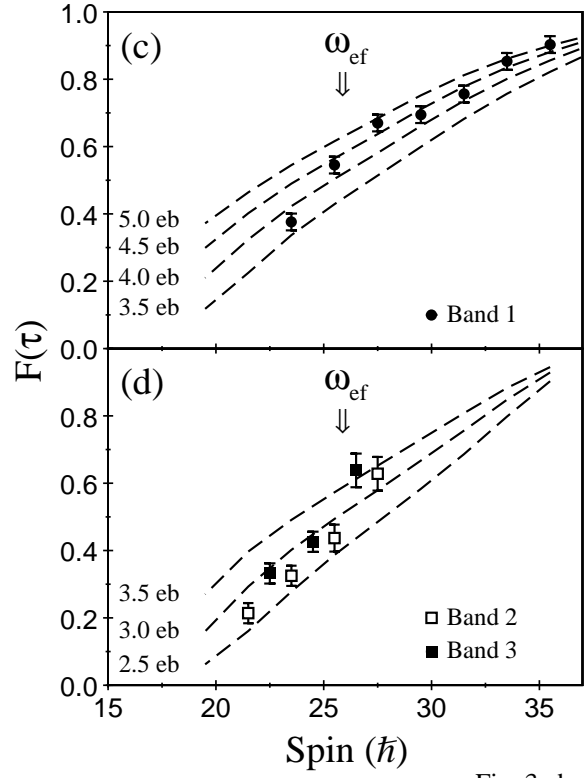
FIG. 3. Forward- (a) and backward-angle (b), double-gated γ-ray spectra for the $(\pi,\alpha) =$ $(-,-1/2)$ band 1 in ^{133}Pr. Above the 922 keV $(43/2^- \to 39/2^-)$ transition only Doppler shifted components are observed and are labelled by their centroid energies in keV. Experimental (data points) and theoretical (dashed curves of constant Q_t) fractional Doppler shift factors for band 1 (c) and bands 2, 3 (d). The spin corresponding to the onset of the ω_{ef} alignment of neutrons is indicated.
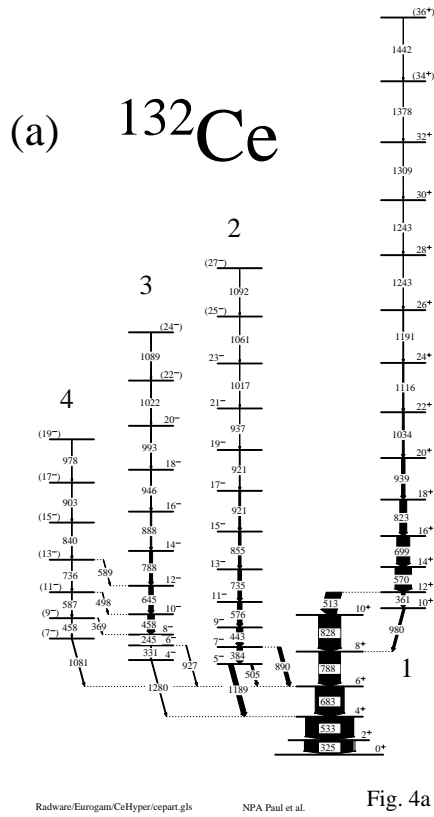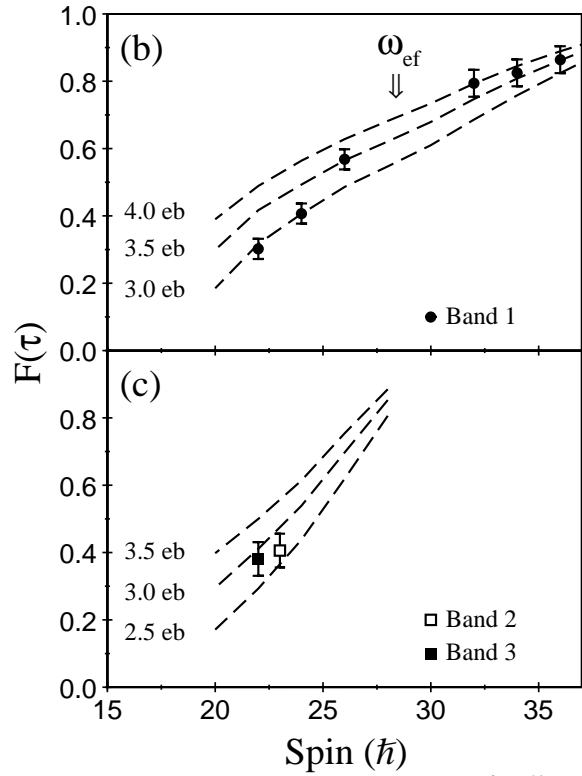
FIG. 4. Partial level scheme for ^{132}Ce [6] (a). The transition energies are given in keV and their relative intensities are proportional to the widths of the arrows. Experimental (data points) and theoretical (curves of constant Q_t) fractional Doppler shift factors for band 1 (b) and bands 2, 3 (c). Experimental points at $I = 28\hbar$ and $I = 30\hbar$ in band 1 have been omitted because the corresponding transitions consist of an exact energy doublet (1243 keV), precluding a meaningful centroid-shift measurement. The spin corresponding to the onset of the ω_{ef} alignment of neutrons is indicated.
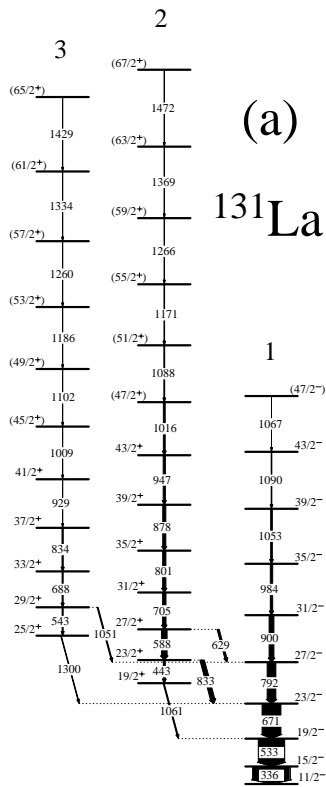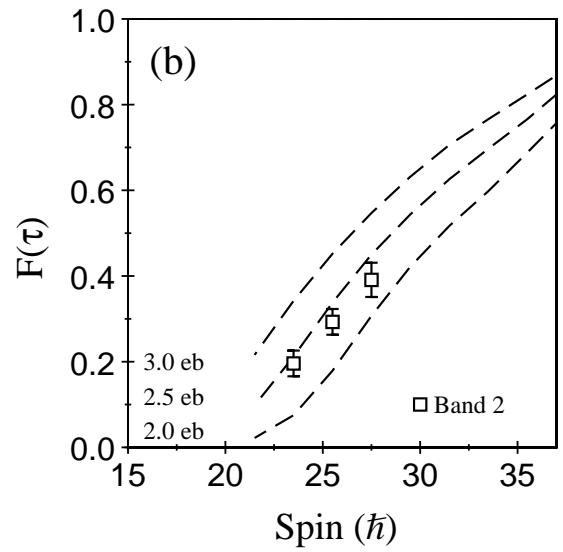
FIG. 5. Partial level scheme for ^{131}La [17] (a). The transition energies are given in keV and their relative intensities are proportional to the widths of the arrows. Experimental (data points) and theoretical (curves of constant Q_t) fractional Doppler shift factors for band 2(b).
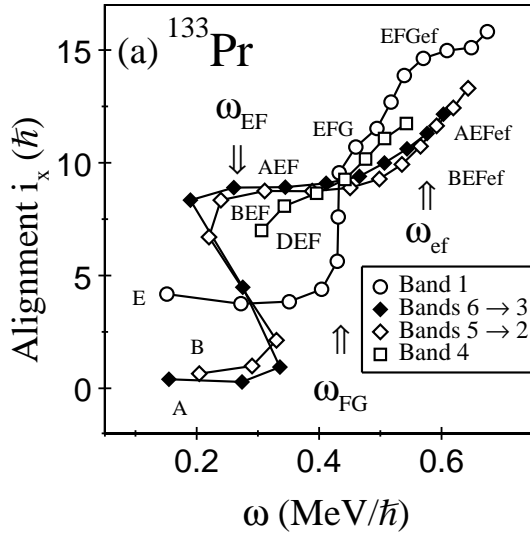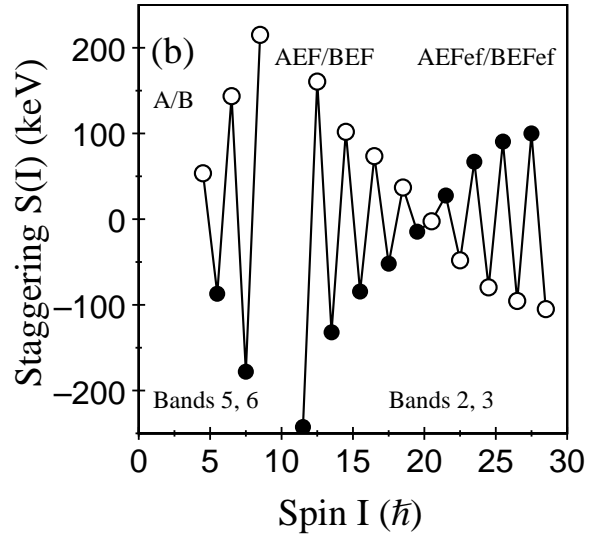
FIG. 6. Experimental alignments for the bands in ^{133}Pr (a) with quasiparticle configurations and rotational alignments labelled. Staggering parameter for the positive-parity signature-partner bands in ^{133}Pr (b). Open circles correspond to $(\alpha = +1/2) \rightarrow (\alpha = -1/2)$ $\Delta I = 1$ transitions, solid circles correspond to $(\alpha = -1/2) \rightarrow (\alpha = +1/2)$ $\Delta I = 1$ transitions.
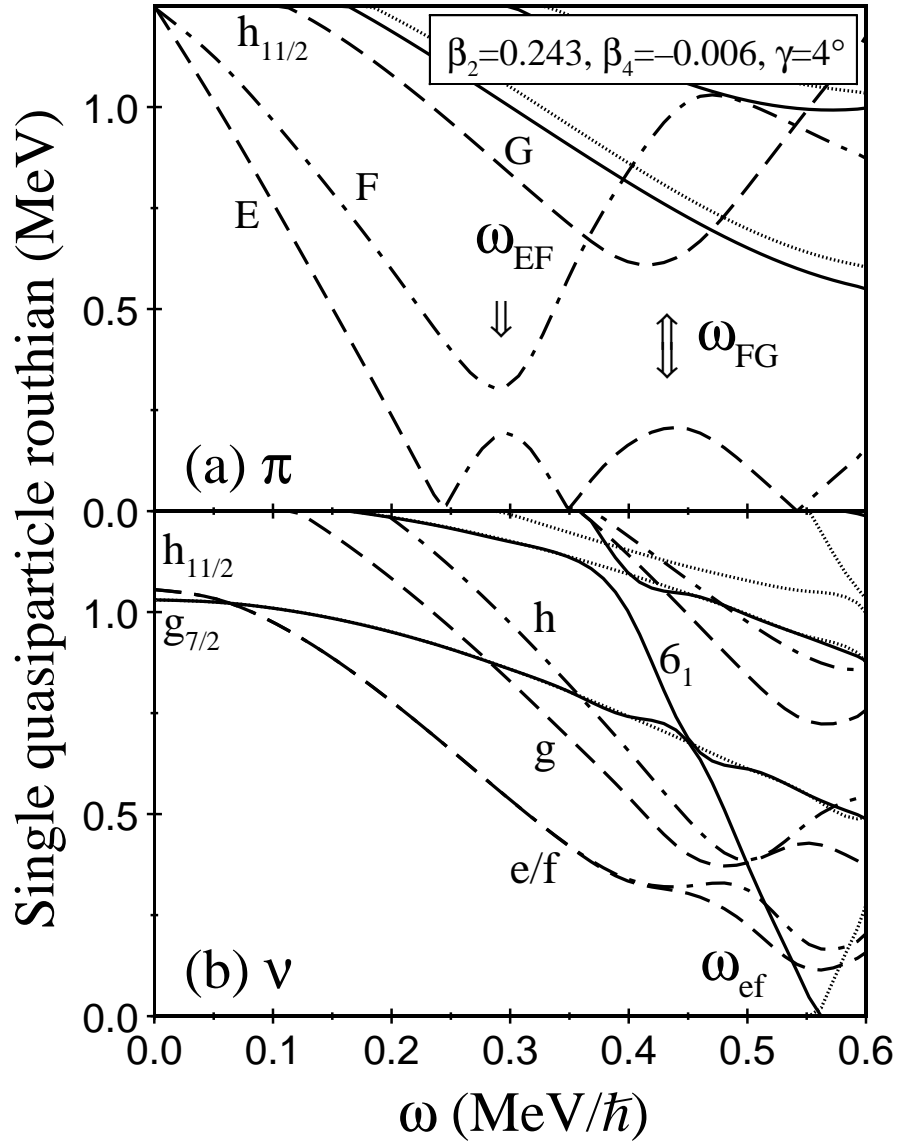
Fig. 7

FIG. 7. Cranked Woods-Saxon single-quasiparticle energies for protons (a) and neutrons (b) calculated at a deformation corresponding to the "enhanced" TRS minimum. The parity and signature (π,α) of the levels are: $(+,+1/2)$ – solid lines; $(+,-1/2)$ – dotted lines; $(-,-1/2)$ – dashed lines; $(-,+1/2)$ – dot-dashed lines. Quasiparticle alignments are indicated. In (b), the g, h and 6_1 orbitals all derive from $\Omega = 1/2$ levels above the N = 82 spherical shell gap.
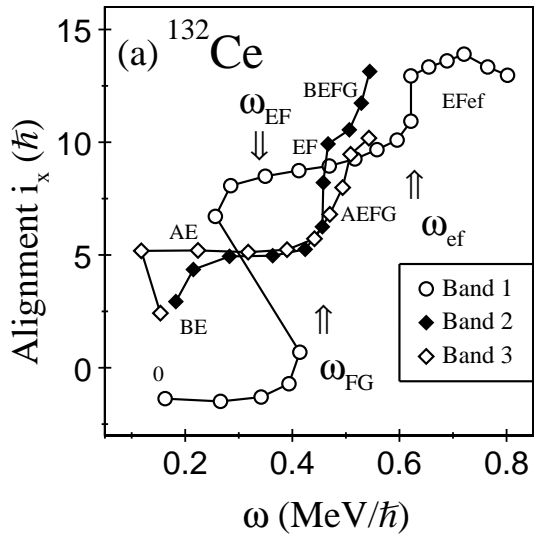
Fig. 8a
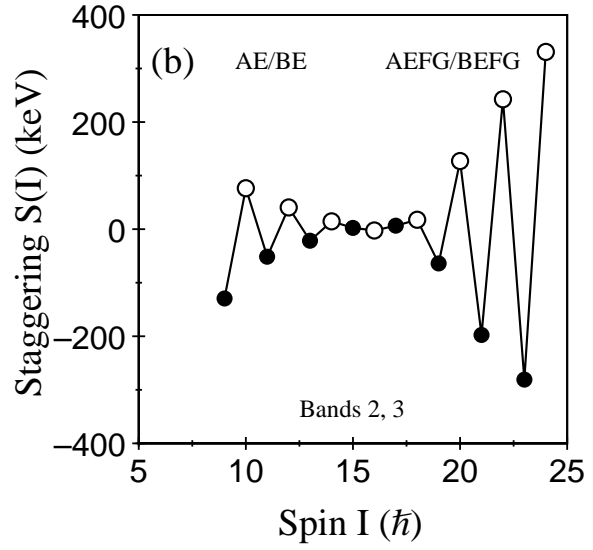
Fig. 8b

FIG. 8. Experimental alignments for the bands in ^{132}Ce (a) with quasiparticle configurations and rotational alignments labelled. Staggering parameter for the negative-parity signature-partner bands in ^{132}Ce (b). Open circles correspond to $(\alpha = 0) \rightarrow (\alpha = 1)$ $\Delta I = 1$ transitions, solid circles correspond to $(\alpha = 1) \rightarrow (\alpha = 0)$ $\Delta I = 1$ transitions.
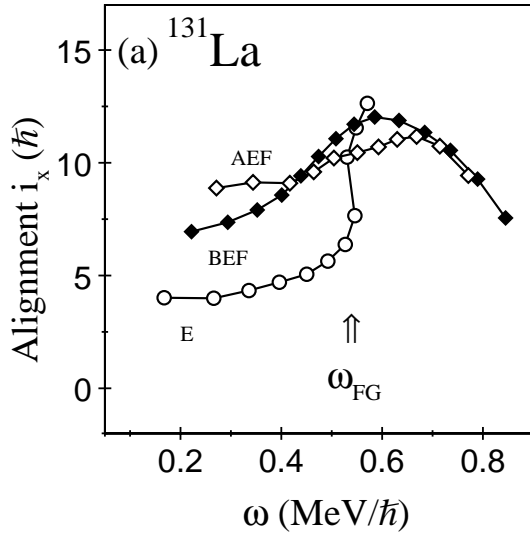
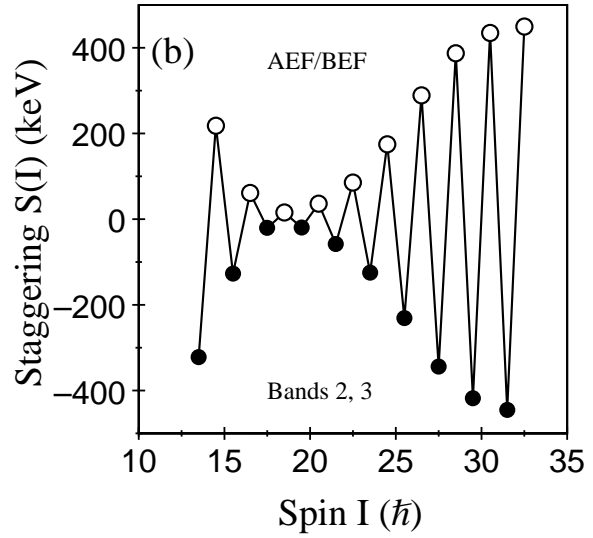FIG. 9. Experimental alignments for the bands in ^{131}La (a) with quasiparticle configurations and rotational alignments labelled. Staggering parameter for the positive-parity signature-partner bands in ^{131}La (b). Open circles correspond to $(\alpha = +1/2) \rightarrow (\alpha = -1/2)$ $\Delta I = 1$ transitions, solid circles correspond to $(\alpha = -1/2) \rightarrow (\alpha = +1/2)$ $\Delta I = 1$ transitions.